






Membrane InGaAsP Mach–Zehnder Modulator Integrated With Optical Amplifier on Si Platform

Tatsuro Hiraki , *Member, IEEE*, Takuma Aihara , *Member, IEEE*, Takuro Fujii , *Member, IEEE*, Koji Takeda , *Senior Member, IEEE*, Takaaki Kakitsuka , *Member, IEEE*, Tai Tsuchizawa, and Shinji Matsuo, *Fellow, IEEE*

Abstract—A high-efficiency Mach-Zehnder modulator (MZM) using InGaAsP phase shifters and a semiconductor optical amplifier (SOA) using multiple-quantum-well (MQW) are integrated on Si-waveguide circuits. Membrane structure is easy to optically couple to the widely-used 220-nm-thick Si waveguides, because both layers have comparable effective refractive indices. To integrate different bandgap III-V compound semiconductors; InGaAsP-based MQW for SOA and InGaAsP bulk for MZM, we employ epitaxial regrowth on thin-InP layer that is directly bonded on a silicon-on-insulator (SOI) wafer. Their thicknesses are smaller than the critical thickness (~ 430 nm) for epitaxial growth of the InP-based layers bonded on the SOI wafer. This fabrication procedure is beneficial for the wafer-level integration of InP-based devices with different bandgaps on Si-photonics circuits. Furthermore, membrane lateral *p-n* and *p-i-n* diode structures improve the modulation efficiency of the MZM and reduce the power consumption of the SOA due to the high optical confinement factor and small active area. The integrated 300- μm -long SOA and MZM with 500- μm -long phase shifters show a fiber-to-fiber lossless operation with the SOA current of only 24 mA at room temperature. The modulation efficiency of the compact MZM is high enough for eye opening with non-return-to-zero (NRZ) signals from 28 to 40 Gbit/s. By using the SOA to amplify the signals modulated by the MZM, the fiber output power of -3.4 dBm was obtained without any significant pattern effect.

Index Terms—Electrooptic modulators, semiconductor optical amplifiers, optoelectronic devices.

I. INTRODUCTION

NETWORK traffic in datacenters is rapidly increasing, so there is a strong demand for large-capacity optical fiber links to provide high-throughput data transmission. The critical issues in meeting this demand are the cost, size, and power

consumption of the large-capacity optical transceivers. A Mach-Zehnder modulator (MZM) is a key component of large-capacity optical transceivers because it provides high baud rates and enables the use advanced modulation formats with both phase and intensity modulation. Recently, Si photonics technology has been used to monolithically integrate MZMs with various compact optical components, such as wavelength filters, polarization splitters and rotators, and photodetectors [1]–[3]. Photonic integrated circuits (PICs) using this technology can reduce the size and assembly cost of optical transceiver modules. However, problems with Si photonics include a large fiber coupling loss, poor modulation efficiency and large absorption loss of the Si MZMs, as well as a lack of integrated optical gain devices such as laser diodes and optical amplifiers. At present, these problems limit the further reductions in the cost, size, and power consumption of optical transceivers.

A promising solution is a heterogeneous integration of III-V semiconductors on a Si platform. InP-based materials provide high-efficiency optical phase modulation and low free-carrier absorption loss [4], [5], which are beneficial for improving MZM performance [5]–[7]. In addition, they also provide a large optical gain due to their direct bandgap and can therefore be used to integrate optical gain devices on a Si platform. The recent progress in the direct wafer bonding method makes it easy to integrate III-V layers on a Si platform [8], [9]. Several types of MZMs, lasers, and SOAs have been demonstrated by using III-V semiconductors on Si [6], [7], [10]–[13]. However, integrating them on Si-waveguide circuits is still challenging. One of the issues is optical coupling between the III-V semiconductor and Si waveguide layers. Typical InP-based vertical diodes have 2–3- μm -thick semiconductor layers, but their effective refractive index is much larger than that of the widely-used 220-nm-thick Si waveguide [12], [14], [15], which makes it difficult to optically couple III-V layers to it. In previous works, the Si layer thickness was increased to 400–500 nm for effective index matching, but such a thick Si layer is not compatible with the widely developed 220-nm-thick Si waveguides. Another issue is the integration of materials with different bandgaps for the MZM and optical gain devices on Si waveguide circuits. A preferable approach to integrate different bandgap materials is using an epitaxial regrowth technique, because this is the same fabrication procedure to fabricate III-V semiconductor-based PICs such as electro-absorption modulator integrated DFB (EA-DFB) laser. In EA-DFB laser, different bandgap materials have been

Manuscript received November 15, 2019; revised January 17, 2020; accepted February 3, 2020. Date of publication March 2, 2020; date of current version May 27, 2020. (*Corresponding author: Tatsuro Hiraki.*)

Tatsuro Hiraki, Takuma Aihara, Takuro Fujii, Koji Takeda, Tai Tsuchizawa, and Shinji Matsuo are with the NTT Device Technology Labs and NTT Nanophotonics Center, NTT Corporation, Atsugi 243-0198, Japan (e-mail: tatsuro.hiraki.gu@hco.ntt.co.jp; takuma.aihara.vp@hco.ntt.co.jp; fujii.uc@hco.ntt.co.jp; koji.takeda.vk@hco.ntt.co.jp; tai.tsuchizawa.ya@hco.ntt.co.jp; shinji.matsuo.vm@hco.ntt.co.jp).

Takaaki Kakitsuka was with the NTT Device Technology Labs, NTT Corporation, Atsugi 243-0198, Japan. He is now with the Graduate School of Information Production and Systems, Waseda University, Kitakyushu 808-0135, Japan (e-mail: t.kakitsuka@waseda.jp).

Color versions of one or more of the figures in this article are available online at <http://ieeexplore.ieee.org>.

Digital Object Identifier 10.1109/JLT.2020.2977426

monolithically integrated on InP wafer by using the epitaxial growth process. However, once a 2–3- μm -thick III-V layer is bonded onto a silicon-on-insulator (SOI) wafer, it is difficult to form different-bandgap materials by epitaxial growth, due to thermal expansion coefficient mismatch between III-V semiconductors and Si. As a result, we have to employ multiple-die bonding of different materials (i.e., micro transfer printing [16], [17]); however, it is not suitable for high-throughput fabrication of a large number of components.

To overcome these problems, the best way to solve the problems is to reduce the III-V layer thickness. When the III-V layer thickness is comparable to the Si layer thickness, the effective refractive index of the III-V layer becomes small enough for optical coupling to Si waveguides [11], [18]. In addition, such III-V layer thickness is much smaller than the critical thickness. Here, the critical thickness (~ 430 nm) is determined by the difference in the thermal expansion coefficients between the III-V layer and Si substrate, as discussed in our previous work [19]. So, materials with various bandgaps can be integrated on Si waveguide circuits by using epitaxial regrowth. In previous work, we have demonstrated epitaxial regrowth of InP layer to fabricate low-power consumption directly modulated lasers [20], [21]. For MZM, we have proposed to use a high-efficiency membrane InGaAsP phase shifters and hydrogen-free SiN waveguides [7], [22], and demonstrated a $V_{\pi}L$ of 0.4 Vcm and error-free operation for 40-Gbit/s NRZ signals [7]. However, the insertion loss, including that of the fiber couplings and MZM, was still large, and the phase shifter had not been integrated with the widely used 220-nm-thick Si-waveguide circuits yet. In this work, we integrated our previously proposed membrane InGaAsP phase shifter with an SOA on 220-nm-thick Si waveguide circuits [23]. To integrate them with the Si waveguide, we employ chemical mechanical polishing (CMP) before bonding InP substrate including multiple-quantum-well (MQW) layer of the SOA. After that we demonstrate the epitaxial regrowth of InGaAsP bulk layer for the phase shifter. Advantage of the membrane SOA is that we can design to compensate for the total optical loss of the fiber couplings and MZM with a low injection current. We describe the characteristics in detail, including the optical gain at room temperature [23] and 80 °C, and dynamic modulation for 28- and 40-Gbit/s NRZ signals for booster amplifier operation.

II. DESIGN AND FABRICATION

Fig. 1(a) shows a top view of the integrated MZM and SOA on 220-nm-thick Si-waveguide circuits [23]. The SOA is 300 μm long. It is integrated with silicon waveguides and connected to the compact MZM, which consists of 2 x 2 Si multimode interferometers (MMIs) and 500- μm long InGaAsP phase shifters. Fiber-chip interfaces are formed from a large 3-x-3- μm^2 silica-based (SiO_x) core. 300- μm -long inverse silicon taper waveguides are used to convert the light from Si core to SiO_x core [1], [24]. The spot-size converter typically provides a low coupling loss (~ 2 dB/facet) and easy butt-coupling to an optical fiber.

Fig. 1(b) shows a cross-sectional view of the SOA. The SOA has an InGaAsP-based six-period MQW core, whose

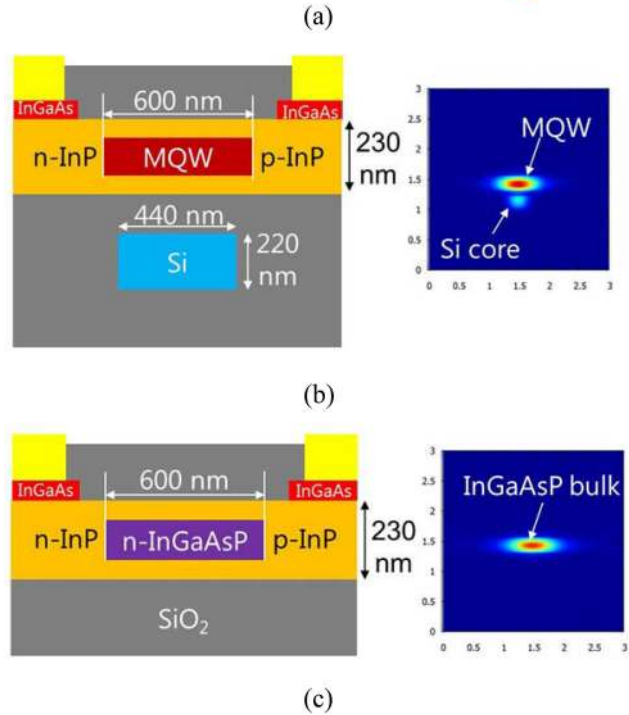
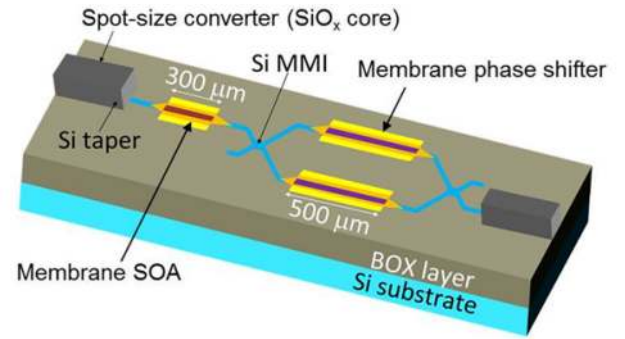


Fig. 1. (a) Bird's eye view of integrated membrane MZM and SOA on Si waveguide circuits [23]. Cross section views and calculated mode field patterns of (b) SOA and (c) phase shifter.

photoluminescence (PL) wavelength is 1.52 μm . The size of the MQW core is 0.6 x 0.1 μm^2 . The core is buried within the 230-nm-thick InP layer, whose thickness is comparable to the Si-layer thickness (220 nm) for effective-refractive-index matching. This device has a lateral current-injection *p-i-n* diode structure. Although there is a tradeoff between the power consumption and saturation output power, in this work, we focused on the low-power-consumption operation. To reduce the current required for the SOA, the small cross-sectional area of the active region and large fill factor in the MQW layer are essential. Thanks to the effective index matching, the fill factor in the MQW can be controlled by changing the Si-core width. Fig. 2 shows the calculated fill factors in the MQW, *p*-InP, and Si with various Si-core widths. The SiO₂ thickness between the III-V and Si layers is 100 nm. The fill factor in the MQW layer increases with decreasing Si width, but almost saturates at the width of less than 400 nm. The fill factors in the *p*-InP and Si core get larger and smaller with decreasing Si width. Since the absorption loss of the *p*-InP is much larger than that of the Si,

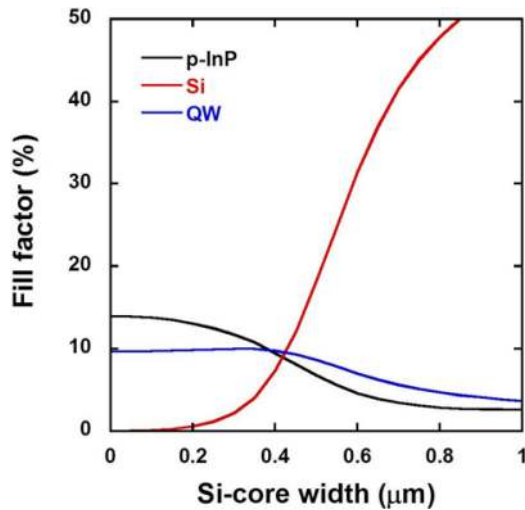


Fig. 2. Calculated fill factor into *p*-type InP, Si core, and MQW layer for various Si-core widths.

the core width should be set to around 400 nm to obtain the largest fill factor in the MQW with a low *p*-InP absorption loss for low-current operation. In this work, we set the Si width to 440 nm, which provides fill factors in the MQW and *p*-InP layers of about 9.4% and 8%, respectively. The change in the fill factor in the MQW is less than $\pm 0.1\%$, when the SiO₂ thickness is varied from 80 to 120 nm.

Fig. 1(c) shows a cross-sectional view of the phase shifter. We used a membrane lateral *p*-*n* diode structure for the carrier-depletion phase shifter proposed in our previous work [6], [7]. The *n*-type InGaAsP core, whose PL peak wavelength is 1.3 μm , is buried within the 230-nm-thick InP layer. The size of the InGaAsP core is $0.6 \times 0.1 \mu\text{m}^2$. Fig. 1(c) also shows an optical mode field pattern of the phase shifter. In the previous work, this type of the membrane InGaAsP phase shifter with the SiN waveguide showed a $V_{\pi}L$ of around 0.4 Vcm due to the high optical confinement factor, and demonstrated 40-Gbaud operation [7]. Thanks to the high modulation efficiency, it provides low-voltage modulation despite the short phase-shifter (500 μm). Here, we simply followed the design of the phase shifter in our previous work, but this design has not been optimized. Ideally, with the high optical confinement factor maintained, the optical loss due to the *p*-type InP region can be reduced further by coupling to the Si core, as described above.

Both the phase shifter and SOA are connected to the $0.22 \times 0.44\text{-}\mu\text{m}^2$ Si waveguide core with reasonably narrow and short InP tapers. Fig. 3 shows a schematic of the taper region between the Si waveguide and SOA. The tip of the InP taper is 100-nm wide. The membrane III-V layer easily couples to the Si waveguide and thus provides very low-loss and short tapers [14]. The calculated taper coupling loss is less than 0.1 dB. In addition, the tip of short membrane taper has a low aspect ratio, which makes the taper easy to fabricate compared with the high-aspect-ratio taper of typical vertical diodes. By using the membrane layer, the low-loss and low-reflection InP taper can be easily fabricated to integrate the SOA on a Si platform.

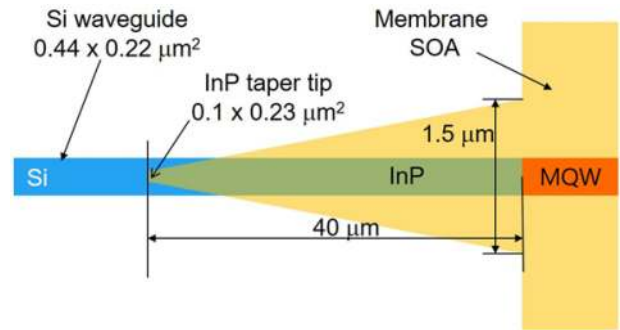


Fig. 3. Schematic of taper between Si waveguide and SOA.

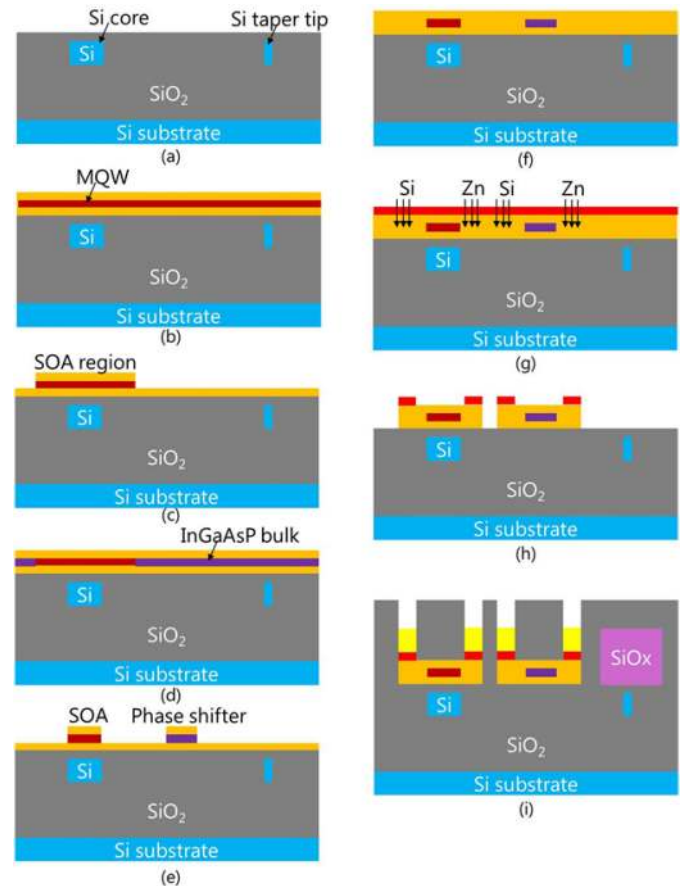


Fig. 4. Fabrication procedure for integrated MZM and SOA.

We fabricated the designed device by combining the direct bonding and epitaxial regrowth, as shown in Fig. 4. First, a Si waveguide layer was patterned on a SOI wafer, whose buried oxide thickness was 2 μm . Next, the SiO₂ cladding film was deposited, followed by CMP [Fig. 4(a)]. Here, the SiO₂ thickness on the Si layer was controlled to be 100 nm. After that, an InP wafer including an InGaAsP MQW layer for the SOA was bonded onto the SOI wafer by using the oxygen-plasma-assisted bonding method [20], [25]. After the removal of the InP substrate [Fig. 4(b)], the MQW layer was removed without reducing the area for the SOA, and the 50-nm-thick InP layer

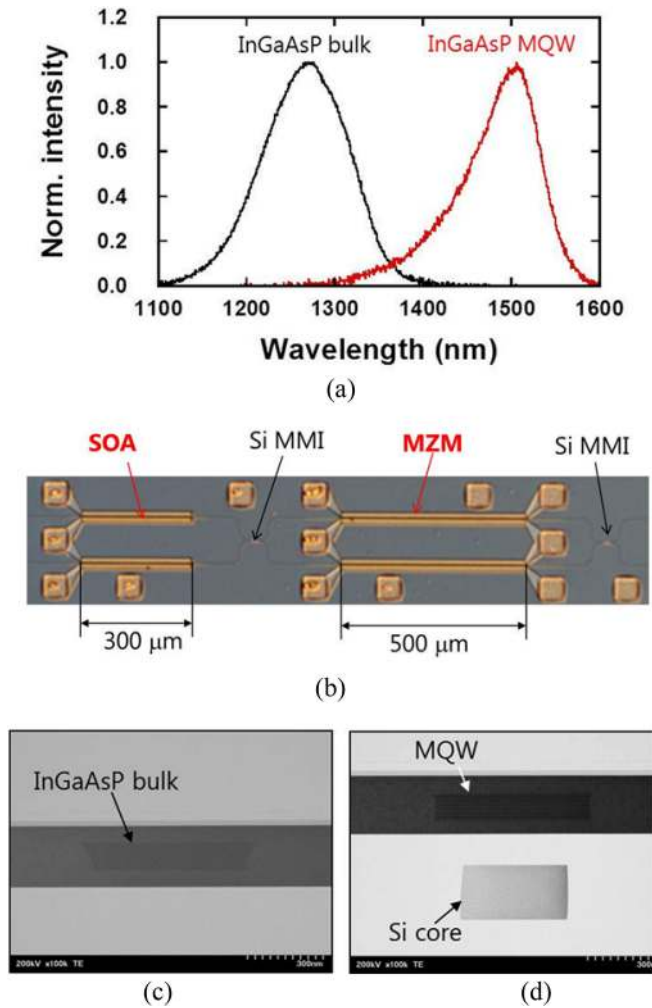


Fig. 5. (a) Micro PL spectrum of fabricated buried cores of phase shifter and SOA [23]. (b) Microscope image of fabricated device [23], and cross sectional TEM images of (c) phase shifter and (d) SOA.

remained on the SiO₂ [Fig. 4(c)]. Then, an n-type InGaAsP bulk layer was regrown on the remaining InP layer at 600 °C [Fig. 4(d)]. After that, the cores for both the SOA and phase shifter were patterned [Fig. 4(e)], followed by regrowth of an InP layer to form the buried heterostructures [Fig. 4(f)]. After growing an InGaAs contact layer, the donor and acceptor regions were formed by Si ion implantation and Zn thermal diffusion, respectively [Fig. 4(g)] [20]. Next, the InGaAs contact layer was patterned, and then the InP tapers and mesa regions were formed [Fig. 4(h)]. Finally, in the backend process, the metal electrodes and SiO_x cores were fabricated [Fig. 4(i)]. Thanks to the membrane structure, the InGaAsP and InP bulk layer were regrown on the SOI wafer without any of the cracks typically caused by thermal expansion during the epitaxial growth process [19]. This is beneficial for wafer-level integration of various III-V devices on Si.

Fig. 5(a) shows a measured micro PL spectrum of the fabricated buried cores of the phase shifter and SOA. Materials with different bandgaps were successfully formed on the SOI wafer by using the epitaxial growth process. Fig. 5(b) shows a microscope image of the fabricated MZM-SOA device. The

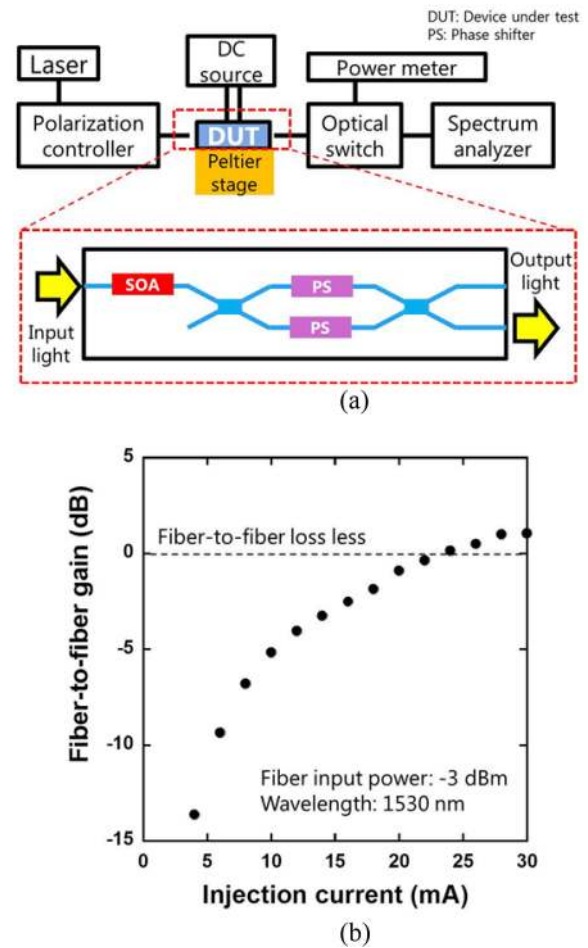


Fig. 6. (a) Experimental setup to measure optical gain and (b) measured fiber-to-fiber gain with various injection currents to SOA.

small footprint of around $1.6 \times 0.3 \text{ mm}^2$ was achieved by using the short phase shifter and InP tapers, and by the heterogeneous integration without a chip assembly process. Fig. 5(c) and (d) shows cross-sectional transmission electron microscope (TEM) images of the fabricated phase shifter and SOA. Even though the buried MQW core is very small, it was precisely aligned with the Si core because the SOA was formed by a wafer-level process using lithography, not a chip assembly process. Thus, by combining wafer bonding and epitaxial growth, we were able to fabricate the membrane devices with the Si waveguide.

III. MEASURED CHARACTERISTICS

A. Amplification of CW Light

First, we characterized the optical gain of the integrated SOA. Fig. 6(a) shows the experimental setup. We input continuous wave (CW) light from a tunable laser diode to the polarization controller, which set the polarization to the transverse electric (TE) mode. The TE-mode light was coupled to the chip and then input to the SOA. The DC bias of the MZM was set to maximize the output power from the cross port. The chip was set onto the stage, whose temperature was controlled by a Peltier cooler. Input and output fibers were lensed fibers. In this work,

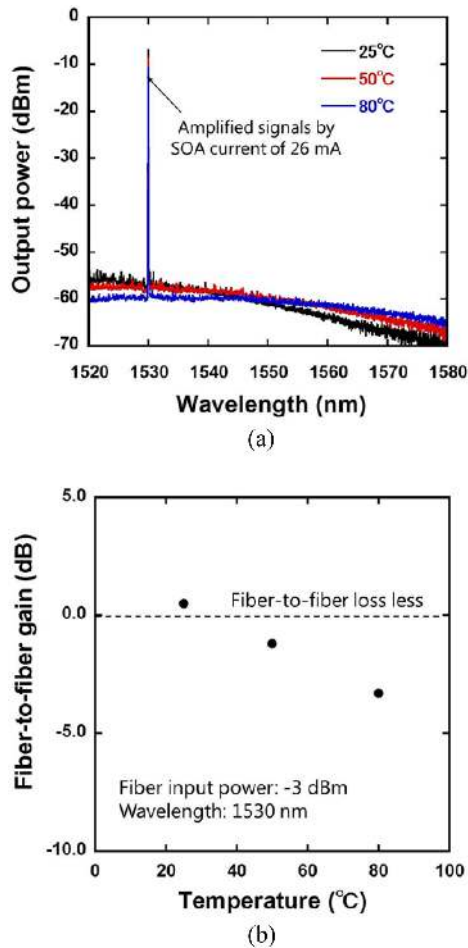


Fig. 7. Measured temperature dependences of (a) output light spectrum and (b) fiber-to-fiber gain at 26 mA.

the fabricated device did not have a phase-tuning heater, and in the experiment, the input wavelength was fixed to 1530 nm. Fig. 6(b) shows the measured injection-current dependence of the fiber-to-fiber gain, which is defined as the gain normalized by the fiber-to-fiber transmission. Here, the fiber input power was -3 dBm and the fiber coupling loss was ~ 2 dB, which was estimated by measuring the transmittance of the reference Si waveguide on the chip. The lossless condition was achieved at an injection current of only around 24 mA and power consumption of around 54 mW. Total optical losses, including those of the MZM and two fiber-chip couplings, are completely compensated by the low injection current, thanks to the membrane structure.

We also characterized the temperature dependence of the optical gain. Fig. 7(a) shows the measured output light spectrum at the injection current of 26 mA at temperatures from 25 to 80 °C. The wavelength of the input light was 1530 nm. At high temperatures, the amplified spontaneous emission (ASE) spectrum was broadened and its peak wavelength was shifted to longer wavelength. Fig. 7(b) shows the measured fiber-to-fiber gain at temperatures from 25 to 80 °C. The SOA injection current and the fiber input power were 26 mA and -3 dBm. The fiber-to-fiber gain slightly degraded with increasing temperature because the material gain of the MQW layer was reduced at high temperatures. However, the total loss was only 3.3 dB even at

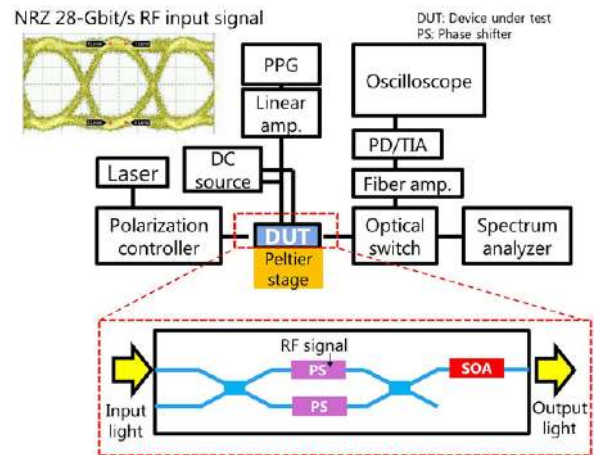


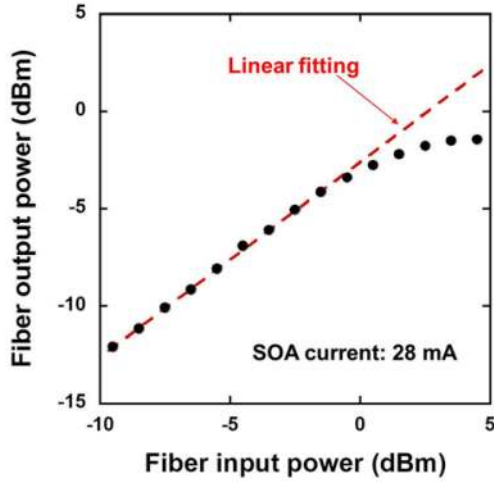
Fig. 8. Experimental setup.

80 °C, which is much lower than that of conventional MZM devices on a Si platform without an integrated SOA. We also achieved the low-loss and low-power-consumption operation at high temperature. Here, the injection current to the SOA was set to prevent the lasing at 25 °C. The lasing was caused mainly by optical reflections at the fiber-chip interface and experimental setup. The optical reflections could be reduced applying butt coupling to the optical fiber and introducing an optical isolator in the setup. Then the loss at high temperature could be reduced by increasing the injection current. Furthermore, from the measured ASE spectrum [(Fig. 7(a))], the gain reduction at high temperature can be suppressed at the longer wavelength than 1530 nm in the C band due to the detuning of the PL wavelength of the MQW layer.

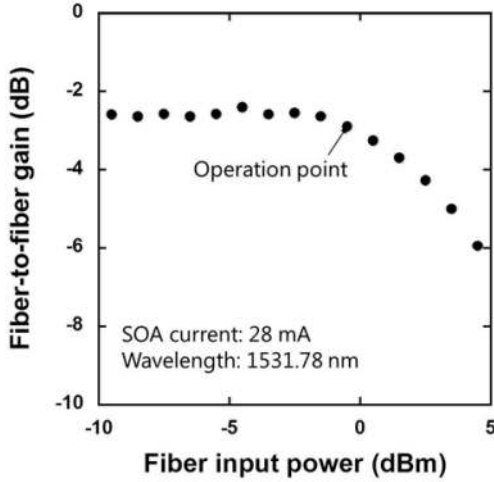
B. Amplification of Modulated Light

Next, we input CW light from the fiber to the MZM and amplified the modulated signals with the integrated SOA. Input light propagates in the opposite direction from that mentioned in the previous section, as shown in Fig. 8. This situation is more practical for the booster amplifier because the amplified signal does not pass through the MZM and thus an output power larger than those mentioned in the previous section can be obtained. However, the signal quality of the output light strongly depends on the fiber input power because of the pattern effect due to the depletion of the injected carriers in the saturated region. Therefore, the operation condition of the SOA must be carefully considered.

Fig. 8 shows the experimental setup for the booster amplifier configuration. The TE-mode CW light was input to the MZM, and then the modulated signals were amplified by the SOA on the chip. The RF signals were generated by the pulse pattern generator (PPG) and fed into the linear amplifier. The monitored amplified signal at NRZ 28 Gbit/s is shown in Fig. 8. The RF signal was input to one arm of the MZM with the DC bias of -2.0 V. The other arm was set to a DC bias of -5.5 V. The output signal from the SOA was coupled to the output fiber and then fed into the photodiode/transimpedance amplifier (PD/TIA) module. Here, the input and output fibers were high numerical



(a)



(b)

Fig. 9. Measured input-power dependence of (a) fiber output power and (b) fiber-to-fiber gain.

aperture fibers, which were butt-coupled to the SiOx core. The modulated signals were measured by the sampling oscilloscope.

First, to check the saturation characteristics of the device, we measured the output power and fiber-to-fiber gain with various fiber input optical powers without RF input. Here, the injection current to the SOA was fixed at 28 mA. Fig. 9(a) and (b) show the measured input-power dependence of the fiber output power and fiber-to-fiber gain. Here, the DC bias of the MZM (-2.0 V) was set for the largest eye amplitude at the wavelength of 1531.78 nm (near the quadrature point), but not for the maximum transmittance of the MZM, as tested in the previous section. Therefore, the measured fiber-to-fiber loss was over zero. As shown in Fig. 9(b), a 3-dB gain reduction was observed at the fiber input power of over $+3.5$ dBm due to the output power saturation. At that power, the fiber-coupled output power was around -1.5 dBm. To prevent the pattern effect of the SOA, we set the input power to -0.5 dBm for the unsaturated region, which means the fiber output power was around -3.4 dBm. The measured eye diagram for 28- and 40-Gbit/s NRZ signals with

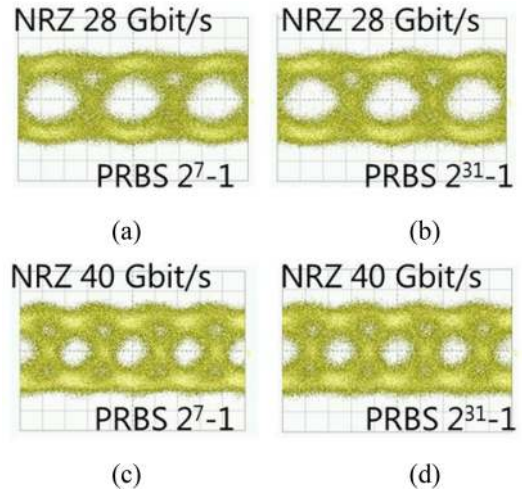


Fig. 10. Measured eye diagrams for NRZ 28-Gbit/s signals with PRBS (a) 2^7-1 and (b) $2^{31}-1$ and NRZ 40-Gbit/s signals with PRBS (c) 2^7-1 and (d) $2^{31}-1$.

pseudo-random bit sequence (PRBS) 2^7-1 and $2^{31}-1$ are shown in Fig. 10(a)–(d), respectively. The input peak-to-peak voltage to one arm of the MZM was $4 V_{pp}$. Since the input power was lower than the saturation power, the eye diagrams for both PRBS 2^7-1 and $2^{31}-1$ were opened without significant pattern effect. We measured the eye diagram using the *p-i-n* diode and obtained the extinction ratio of ~ 10 dB at NRZ 28 Gbit/s with $4 V_{pp}$, even though the phase shifter length was only $500 \mu\text{m}$. The result is almost consistent with the previous results [7] and indicates that the integrated MZM has high modulation efficiency. The high efficiency MZM was integrated with the SOA by using the direct wafer bonding and epitaxial growth of the InGaAsP-bulk layer on the Si-waveguide circuits.

In this work, the measured saturation output power was not so large, because the large fill factor and small cross-sectional area of the MQW core were designed for low-power-consumption operation, which is suitable for short-link applications. These parameters must be changed depending on the target applications. For the large saturation output power, reducing the fill factor and increasing the active area are necessary.

IV. CONCLUSION

We described an integrated high-efficiency membrane InGaAsP MZM with an MQW SOA on Si-waveguide circuits. The membrane lateral *p-n* and *p-i-n* diode structures were beneficial for optical coupling to widely-used 220-nm-thick Si waveguides and epitaxial growth of materials with different bandgaps on the SOI wafer. The optical gain of the fabricated device is large enough for low fiber-to-fiber loss with the SOA current of only 24 mA, and the fiber-to-fiber loss is only 3.3 dB even at 80°C at 26 mA. In addition, the SOA amplified the optical signals, modulated by the integrated MZM, at NRZ 28 and 40 Gbit/s for both PRBS 2^7-1 and $2^{31}-1$. This technology has a potential to reduce the cost, size, and power consumption of large-capacity optical transceivers.

REFERENCES

- [1] T. Tsuchizawa *et al.*, "Microphotonics devices based on silicon micro-fabrication technology," *IEEE J. Select. Quant. Electron.*, vol. 11, no. 1, pp. 232–240, Jan./Feb. 2005.
 - [2] H. Fukuda, K. Yamada, T. Tsuchizawa, T. Watanabe, H. Shinojima, and S. Itabashi, "Silicon photonic circuit with polarization diversity," *Opt. Express*, vol. 16, no. 7, pp. 4872–4880, Mar. 2008.
 - [3] R. Soref and B. Bennett, "Electrooptical effects in silicon," *IEEE J. Quantum Electron.*, vol. 23, no. 1, pp. 123–129, Jan. 1987.
 - [4] B. R. Bennett, R. A. Soref, and J. A. Del Alamo, "Carrier-induced change in refractive index of InP, GaAs and InGaAsP," *IEEE J. Quantum Electron.*, vol. 26, no. 1, pp. 113–122, Jan. 1990.
 - [5] T. Hiraki *et al.*, "Heterogeneously integrated III–V/Si MOS capacitor Mach–Zehnder modulator," *Nat. Photon.*, vol. 11, pp. 482–485, Jul. 2017.
 - [6] T. Aihara *et al.*, "56-Gbit/s operations of Mach–Zehnder modulators using 300- μm -long membrane InGaAsP phase shifters and SiN waveguides on Si," in *Proc. Opt. Fiber Commun. Conf. Exhib.*, San Diego, CA, USA, 2019, Paper M4A.3.
 - [7] T. Hiraki *et al.*, "Membrane InGaAsP Mach–Zehnder modulator with SiN:D waveguides on Si platform," *Opt. Express*, vol. 27, no. 13, pp. 18612–18619, Jun. 2019.
 - [8] Q.-Y. Tong, Q. Gan, G. Hudson, G. Fountain, and P. Enquist, "Low temperature InP/Si wafer bonding," *Appl. Phys. Lett.*, vol. 84, no. 5, pp. 732–734, Jan. 2004.
 - [9] D. Liang *et al.*, "Uniformity study of wafer-scale InP-to-silicon hybrid integration," *Appl. Phys. A*, vol. 103, pp. 213–218, Apr. 2011.
 - [10] H. Chen, Y. Kuo, and J. E. Bowers, "A hybrid silicon–AlGaInAs phase modulator," *IEEE Photon. Technol. Lett.*, vol. 20, no. 23, pp. 1920–1922, Dec. 2008.
 - [11] T. Aihara *et al.*, "Lateral current injection membrane buried heterostructure lasers integrated on 200-nm-thick Si waveguide," in *Proc. Opt. Fiber Commun. Conf. Exhib.*, San Diego, CA, USA, 2018, Paper W3F.4.
 - [12] M. Davenport, S. Skendzic, N. Volet, J. Hulme, M. Heck, and J. E. Bowers, "Heterogeneous silicon/III–V semiconductor optical amplifiers," *IEEE J. Select. Quant. Electron.*, vol. 22, no. 6, Nov./Dec. 2016, Art. no. 3100111.
 - [13] T. Hiraki *et al.*, "Heterogeneously integrated low-power-consumption semiconductor optical amplifier on Si platform," in *Proc. Conf. Lasers and Electro-Opt.*, San Jose, CA, USA, 2019, Paper STh3N. 1.
 - [14] T. Aihara *et al.*, "Membrane buried-heterostructure DFB laser with an optically coupled III–V/Si waveguide," *Opt. Express*, vol. 27, no. 25, pp. 36438–36448, Dec. 2019.
 - [15] P. Dong *et al.*, "Novel integration technique for silicon/III–V hybrid laser," *Opt. Express*, vol. 22, no. 22, pp. 26854–26861, Nov. 2014.
 - [16] J. Zhang *et al.*, "Transfer-printing-based integration of a III–V-on-silicon distributed feedback laser," *Opt. Express*, vol. 26, no. 7, pp. 8821–8830, Apr. 2018.
 - [17] H. H. Chang, Y. H. Kuo, R. Jones, A. Barkai, and J. Bowers, "Integrated hybrid silicon triplexer," *Opt. Express*, vol. 18, no. 23, pp. 23891–23899, Nov. 2010.
 - [18] T. Hiraki *et al.*, "III–V/Si integration technology for laser diodes and Mach–Zehnder modulators," *J. J. Appl. Phys.*, vol. 58, Mar. 2019, Art. no. SB0803.
 - [19] T. Fujii, T. Sato, K. Takeda, K. Hasebe, T. Kakitsuka, and S. Matsuo, "Epitaxial growth of InP to bury directly bonded thin active layer on SiO₂/Si substrate for fabricating distributed feedback lasers on silicon," *IET Optoelectron.*, vol. 9, no. 4, pp. 151–157, Jun. 2015.
 - [20] S. Matsuo, T. Fujii, K. Hasebe, K. Takeda, T. Sato, and T. Kakitsuka, "Directly modulated buried heterostructure DFB laser on SiO₂/Si substrate fabricated by regrowth of InP using bonded active layer," *Opt. Express*, vol. 22, no. 10, pp. 12139–12147, 2014.
 - [21] T. Fujii *et al.*, "Heterogeneously integrated membrane lasers on Si substrate for low operating energy optical links," *IEEE J. Select. Quant. Electron.*, vol. 24, no. 1, Jan./Feb. 2018, Art. no. 17424513.
 - [22] T. Hiraki, T. Aihara, H. Nishi, and T. Tsuchizawa, "Deuterated SiN/SiON waveguides on Si platform and their application to C-band WDM filters," *IEEE Photon. J.*, vol. 9, no. 5, Oct. 2017, Art. no. 2500207.
 - [23] T. Hiraki *et al.*, "Loss-less operation of membrane III–V semiconductor Mach–Zehnder modulator with optical amplifier on Si platform," in *Proc. 45th Eur. Conf. Opt. Commun.*, Dublin, Ireland, 2019, Paper Tu.2.A.2.
 - [24] T. Hiraki *et al.*, "Si–Ge–silicon monolithic integration platform and its application to a 22-Gbit/s x 16-ch WDM receiver," *IEEE Photon. J.*, vol. 5, no. 4, Aug. 2013, Art. no. 4500497.
 - [25] D. Liang *et al.*, "Low-temperature, strong SiO₂–SiO₂ covalent wafer bonding for III–V compound semiconductors-to-silicon photonic integrated circuits," *J. Electron. Mater.*, vol. 37, no. 10, pp. 1552–1559, Oct. 2008.
- Tatsuro Hiraki** (Member, IEEE) received the B.E., M.E., and Ph.D. degrees in engineering from Tohoku University, Sendai, Japan, in 2009, 2011, and 2017, respectively. In 2011, he joined NTT Microsystem Integration Laboratories, Nippon Telegraph and Telephone Corporation, Tokyo, Japan. His current research interests include heterogeneously integrated III–V semiconductor Mach–Zehnder modulators, optical amplifiers, and laser diodes on Si photonics circuits. He is a member of the Institute of Electronics, Information and Communication Engineers and The Japan Society of Applied Physics.
- Takuma Aihara** (Member, IEEE) was born in Akita, Japan in 1987. He received the B.E., M.E., and Ph.D. degrees in electrical and electronic information engineering from the Toyohashi University of Technology, Toyohashi, Japan, in 2010, 2012, and 2015, respectively. He joined NTT Device Technology Laboratories in 2015. His research interest includes the III–V semiconductor lasers on Si photonic integrated circuits. Dr. Aihara is a member of The Japanese Society of Applied Physics (JSAP).
- Takuro Fujii** (Member, IEEE) was born in Kyoto, Japan in 1986. He received the B.E. and M.E. degrees in system design engineering from Keio University, Tokyo, Japan, in 2010 and 2012, respectively. He joined NTT Photonics Laboratories in 2012. His research interests include MOVPE growth of III–V semiconductors and the development of III–V semiconductor lasers on Si for photonic integrated circuits. Mr. Fujii is a member of the Institute of Electronics, Information and Communication Engineers, and The Japanese Society of Applied Physics (JSAP). He was the recipient of the Young Scientist Presentation Award from the JSAP in 2014.
- Koji Takeda** (Senior Member, IEEE) received the B.S., M.S., and Ph.D. degrees in electronics engineering from The University of Tokyo, Tokyo, Japan, in 2005, 2007, and 2010, respectively. From 2008 to 2010, he received research fellowship for young scientists from Japan Society for the Promotion of Science. In 2010, he joined NTT Photonics Laboratories. In 2018, he was also with IHP microelectronics GmbH as a Visiting Researcher. His current research interests include ultralow-power optical interconnect, photonic integrated circuit, and photonic crystal lasers. Dr. Takeda is a member of the IEICE and the JSAP. He is the recipient of the Best Student Paper Award from the IEEE Photonics Society in 2009, the Outstanding Student Presentation Award from JSAP in 2010, and the Best Paper Award from IEICE in 2012.
- Takaaki Kakitsuka** (Member, IEEE) was born in Kumamoto, Japan, in 1971. He received the B.S. and M.S. degrees in physics, and the Dr. Eng. degree from Kyushu University, Fukuoka, Japan, in 1994, 1996, and 2012, respectively. In 1996, he joined NTT Opto-Electronics Laboratories, Nippon Telegraph and Telephone Corporation, Tokyo, Japan. In 2019, he became an Associate Professor with the Graduate School of Information, Production and Systems, Waseda University, Fukuoka, Japan. His current research interests focus on semiconductor lasers and their information communication system applications. From 1996 to 2019, his research interests included research on semiconductor lasers and optical integrated devices with NTT Corporation. Dr. Kakitsuka is a member of the IEICE, JSAP, and the Physical Society of Japan.
- Tai Tsuchizawa** received the B.S. and M.S. degrees in physics from Sophia University, Tokyo, Japan, in 1984 and 1986, respectively, and the Ph.D. degree from the University of Tokyo, Japan, in 1990. Currently, he is a Distinguished Laboratory Specialist with NTT Device Technology Laboratories, Atsugi, Japan. In NTT's laboratories, he has engaged in studies on ECR plasma and its application to etching process for microfabrication. He is currently engaged in studies on the fabrication technology for silicon-based optoelectronics devices. Dr. Tsuchizawa is a Member of the Japan Society of Applied Physics.
- Shinji Matsuo** (Fellow, IEEE) received the B.E. and M.E. degrees in electrical engineering from Hiroshima University, Hiroshima, Japan, and the Ph.D. degree in electronics and applied physics from the Tokyo Institute of Technology, Tokyo, Japan, in 1986 and 1988, and 2008, respectively. In 1988, he joined NTT Opto-electronics Laboratories, Atsugi, where he was engaged in research on photonic functional devices using MQW-pin modulators and VCSELs. In 1997, he researched optical networks using WDM technologies with NTT Network Innovation Laboratories, Yokosuka. His research interests include InP-based photonic integrated circuits with NTT Photonics Laboratories and NTT Device Technology Laboratories, Atsugi. Dr. Matsuo is a member of The Japan Society of Applied Physics, and the Institute of Electronics, Information, Communication Engineers of Japan.